Ueda et al. Progress in Earth and Planetary Science (2016) 3:35
DOI 10.1186/s40645-016-0111-8

Progress in Earth and Planetary Science

RESEARCH ARTICLE Open Access

Reactions between komatiite and CO_2-rich seawater at 250 and 350 °C, 500 bars: implications for hydrogen generation in the Hadean seafloor hydrothermal system

Hisahiro Ueda[1,2*], Takazo Shibuya[2,3,4], Yusuke Sawaki[1], Masafumi Saitoh[2,3,4], Ken Takai[2,3,4,5] and Shigenori Maruyama[6]

Abstract

To understand the chemical nature of hydrothermal fluids in the komatiite-hosted seafloor hydrothermal system in the Hadean, we conducted two hydrothermal serpentinization experiments involving synthetic komatiite and a CO_2-rich acidic NaCl fluid at 250 and 350 °C, 500 bars. During the experiments, the komatiites were strongly carbonated to yield iron-rich dolomite (3–9 wt.% FeO) at 250 °C and calcite (<0.8 wt.% FeO) at 350 °C, respectively. The carbonation of komatiites suppressed H_2 generation in the fluids. The steady-state H_2 concentrations in the fluid were approximately 0.024 and 2.9 mmol/kg at 250 and 350 °C, respectively. This correlation between the Fe content in carbonate mineral and the H_2 concentration in the fluid suggests that the incorporation of ferrous iron into the carbonate mineral probably limited magnetite formation and consequent generation of hydrogen during the serpentinization of komatiites. The H_2 concentration of the fluid at 350 °C corresponds to that of modern H_2-rich seafloor hydrothermal systems, such as the Kairei hydrothermal field, where hydrogenotrophic methanogens dominate in the prosperous microbial ecosystem. Accordingly, the high-temperature serpentinization of komatiite would provide the H_2-rich hydrothermal environments that were necessary for the emergence and early evolution of life in the Hadean ocean. In contrast, H_2-rich fluids may not have been generated by serpentinization at temperatures below 250 °C because carbonate minerals become more stable with decreasing temperature in the komatiite-H_2O-CO_2 system.

Keywords: Komatiite, CO_2-rich condition, Early Earth, Hydrothermal alteration, Serpentinization

Introduction

Deep-sea hydrothermal environments have been considered as a favorable environment for the emergence and early evolution of life on Earth (e.g., Yanagawa and Kojima 1985; Russell and Hall 1997). In particular, H_2-rich hydrothermal fluids generated through the serpentinization of ultramafic rocks would have driven prebiotic chemical evolution and the development of biotic energy metabolisms (Takai et al. 2006; Amend and McCollom 2009; Russell et al. 2014; Nakamura and Takai 2014; Shibuya et al. 2016). Molecular hydrogen (H_2) generation during serpentinization is caused by the reduction of water in conjunction with the oxidation of ferrous iron in silicates. This process is written as the following simplified reaction (e.g., Allen and Seyfried 2003; Seyfried et al. 2007; McCollom and Bach 2009):

$$2(\mathrm{FeO})_{\mathrm{rock}} + \mathrm{H_2O} \rightarrow (\mathrm{Fe_2O_3})_{\mathrm{rock}} + \mathrm{H_2},$$

where the ferric iron-bearing solid phase generally precipitates as magnetite (Fe_3O_4). Therefore, H_2 generation is strongly related to magnetite formation during serpentinization (McCollom and Bach 2009).

Among the various prospects for the seafloor hydrothermal systems in the early Earth (e.g., Kump and Seyfried

* Correspondence: ueda.h.ai@m.titech.ac.jp
[1]Department of Earth and Planetary Sciences, Tokyo Institute of Technology, 2-12-1 Ookayama, Meguro-ku, Tokyo 152-8551, Japan
[2]Laboratory of Ocean-Earth Life Evolution Research (OELE), Japan Agency for Marine-Earth Science and Technology (JAMSTEC), 2-15 Natsushima-cho, Yokosuka 237-0061, Japan
Full list of author information is available at the end of the article

2005; Shibuya et al. 2010), two types of serpentinization are hypothesized to be dominant in the Hadean ocean: a komatiite-hosted high-temperature type at oceanic islands/plateaus (Takai et al. 2006; Yoshizaki et al. 2009; Shibuya et al. 2015) and a low-temperature alkaline type hosted by komatiites or peridotites at off-ridge ocean floors (e.g., Russell et al. 2010, 2014; Shibuya et al. 2016). Based on the geological records, Archean oceanic crust was likely much thicker than modern equivalents owing to the higher potential mantle temperature at that time (Ohta et al. 1996; Komiya et al. 2002; Komiya 2004; Moores 2002; Shibuya et al. 2012). This thick lid of oceanic crust probably limited the exposure of mantle peridotites on the seafloor, thus suggesting that komatiite volcanism would have been much more abundant than the exposed mantle peridotites that are frequently observed near modern slow-spreading ridges without a sufficient magmatic supply (Takai et al. 2006). Therefore, it has been pointed out that H_2-rich seafloor hydrothermal environments would have been predominantly driven by komatiite volcanism in the Hadean ocean (Takai et al. 2006). On the other hand, the low-temperature alkaline type could provide distinctive chemical environments such as large pH gradients in the seawater-hydrothermal fluid mixing zones, which may also have been advantageous for the possible development of proton-motive energy metabolisms (Russell et al. 2014; Shibuya et al. 2016).

Previously, hydrothermal alteration experiments have been conducted to understand the potential of H_2 generation during the serpentinization of komatiites under CO_2-free conditions (Yoshizaki et al. 2009; Shibuya et al. 2015; Suzuki et al. 2015). However, as suggested by theoretical calculations (Walker 1985; Kasting 1993; Sleep and Zahnle 2001) and geological records (Lowe and Tice 2004; Ohmoto et al. 2004; Shibuya et al. 2007, 2012, 2013a), the atmospheric CO_2 levels in the early Earth were likely much higher than the modern level. Furthermore, it has been experimentally demonstrated that carbonate formation during the serpentinization of olivine under CO_2-rich conditions suppresses H_2 generation in fluids (Jones et al. 2010; Klein and McCollom 2013; Neubeck et al. 2014). Recently, some experiments have been conducted in komatiite-CO_2-H_2O systems (Lazar et al. 2012; Hao and Li 2015), but H_2 generation in fluids was not the objective in these studies. Therefore, the potential for hydrogen generation through the serpentinization of komatiites in the Hadean has not yet been experimentally evaluated under CO_2-rich conditions.

In this study, we conducted two experiments that simulate the reactions between komatiite and CO_2-rich seawater at 250 and 350 °C, 500 bars, using a batch-type (closed system) hydrothermal reactor (Yoshizaki et al. 2009). The experiments revealed the chemical composition of high-temperature hydrothermal fluids and CO_2 absorption ability of komatiite through serpentinization under CO_2-rich conditions. The results demonstrate the significance of komatiite-hosted hydrothermal systems for seawater chemistry and provide insight into the H_2-rich hydrothermal environments in the CO_2-rich Hadean ocean.

Methods/Experimental

Synthesis of komatiite

The komatiite used in the experiments was synthesized from a mixture of 12 reagents (SiO_2, TiO_2, Al_2O_3, Fe_2O_3, MnO, MgO, $CaCO_3$, Na_2CO_3, K_2CO_3, P_2O_5, NiO, and Cr_2O_3). The chemical composition of the mixed reagents was adjusted to Al-depleted (Barberton-type) komatiite (Smith et al. 1980; Wei et al. 1990; Yoshizaki et al. 2009) because the volcanism of Al-depleted komatiite was likely more predominant than Al-undepleted komatiite in the Hadean (Shibuya et al. 2015). The mixed powder was placed in a Pt-Rh crucible at 1000 °C for 1 h in an electronic furnace to decarbonate the reagents. The mixture was melted at 1600 °C for 0.5 h at the oxygen fugacity of quartz-fayalite-magnetite (QFM) buffer regulated by a H_2-CO_2 gas mixture (Canil 1997). To create a spinifex texture of olivine, the temperature was lowered to 1450 °C over 1.5 h. Next, the crucible was quenched to room temperature, thus yielding a fresh spinifex-textured komatiite (Fig. 1). The composition and texture of the synthetic komatiite and its mineral/glass phases were analyzed using X-ray diffraction (XRD), X-ray fluorescence (XRF), and an electron probe microanalyzer (EPMA) (Table 1). In the interstitial glass, dendritic olivine crystals configurate a spinifex texture. Broadly depending on size, these crystals have Mg# values ranging from 89 to 94. Small amounts of chromian spinels are disseminated in the vicinity of the olivine crystals. Owing to such a mineral assemblage, almost all Ca in the komatiite was partitioned into the interstitial glass (Fig. 1 and Table 1). The synthesized komatiite was crushed in a tungsten mortar and sieved to obtain a <100 μm powder. To remove any contamination of organic materials during sample preparation, the powdered komatiite was washed with acetone and distilled water several times and dried for 12 h in an oven at 50 °C.

Experimental system

The Inconel alloy autoclave used for the hydrothermal alteration experiment is based on the study by Seyfried et al. (1979). It resists corrosion and withstands high-temperature and high-pressure conditions (up to 600 °C and 600 bars; Fig. 2). The reaction cell is made of a gold bag with a titanium head because of the resistance of these materials to high-temperature fluids. Furthermore,

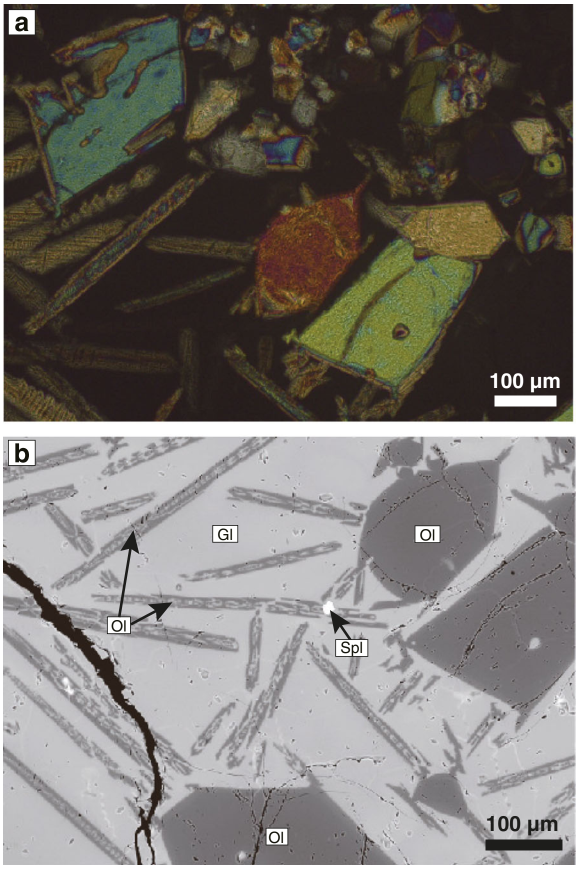

Fig. 1 **a** Photomicrograph taken in cross-polarized light and **b** a backscattered electron (BSE) image of the synthetic komatiite. *Ol* olivine, *Spl* spinel, *Gl* glass

Table 1 Compositions of the synthetic komatiite, mineral/glass phases therein, starting materials used in a previous experiment (wt.%)

Sample	Al-depleted komatiite	Olivine	Glass	Spinel	Basalt[b]
SiO_2	46.29	41.02	50.74	0.22	49.84
TiO	0.37	0.00	0.68	0.22	0.73
Al_2O_3	4.30	0.20	7.74	6.43	15.82
Cr_2O_3	0.21	0.48	0.52	52.22	–
FeO_{total}[a]	12.52	9.70	14.81	22.03	11.00
MnO	0.13	0.09	0.18	0.14	0.22
MgO	27.47	48.80	12.57	15.49	9.44
CaO	7.20	0.30	11.84	0.22	10.84
Na_2O	0.06	0.00	0.23	0.00	1.88
K_2O	0.02	0.02	0.05	0.02	0.18
NiO	0.11	0.34	0.01	0.22	–
Total	98.68	100.95	99.37	97.23	99.95
Mg#[c]	79.64	89.96	60.21	55.62	60.47

–, no mention
[a]Total iron as FeO
[b]Synthetic basalt used in Shibuya et al. (2013b)
[c]Mg# = [Mg / (Mg+Fe)] × 100

gold has sufficient flexibility to allow the fluid inside the reaction cell to be pressurized by the surrounding water. In addition, to avoid possible H_2 generation via the reaction of metallic titanium with water, the surface of the titanium was completely oxidized before the experiments. To eliminate organic contamination, all materials in contact with the reacting fluid were baked in a muffle furnace at 450 °C for 5 h.

The initial solution used in the experiments was controlled at pH 4.9 and 400 mmol/kg of ΣCO_2 ($=CO_{2\,(aq)} + HCO_3^- + CO_3^{2-}$) by the addition of $NaHCO_3$, NaCl, and HCl to ultrapure water, according to the previous studies suggesting that Hadean seawater was acidic due to the high partial pressure of CO_2 in the atmosphere (e.g., Kasting 1993; Macleod et al. 1994). To avoid the degassing of CO_2 by a reaction between $NaHCO_3$ and HCl prior to the sealing of the reaction cell, these materials were separately placed in the gold tube and then mixed after sealing (Shibuya et al. 2013b). The Cl concentration of the solution was regulated to be approximately 1000 mmol/kg because salinity of seawater in the early Earth was potentially 1.5–2 times higher than the modern value (approximately 550 mmol/kg) because of the absence of continents and the associated salt deposits/saline water (Knauth 2005). The komatiite powder was reacted with this hypothetical seawater in the reaction cell at 250 and 350 °C, 500 bars for 1530–2760 h (hereafter abbreviated as Exp-250 and Exp-350, respectively). At the

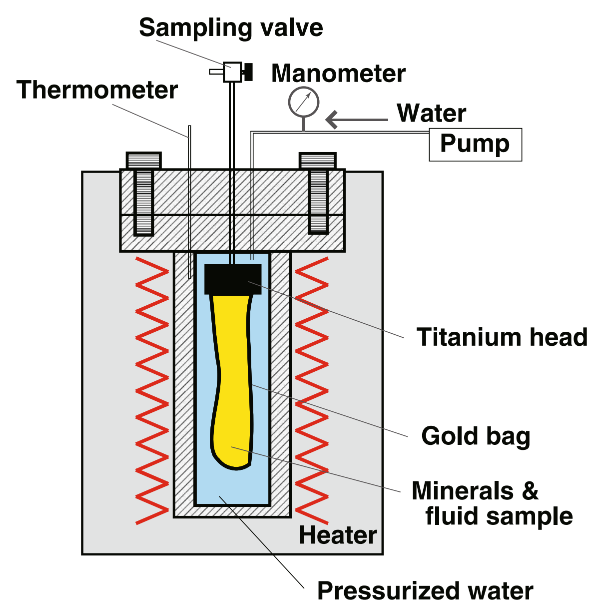

Fig. 2 Schematic illustration of the Inconel alloy autoclave used in this study (modified after Yoshizaki et al. 2009). The synthesized komatiite and hypothetical Hadean seawater were sealed in the gold bag

beginning of the experiments, the water/rock mass ratios were adjusted to approximately 5 because water/rock ratios are commonly below 5 in the high-temperature regions of natural subseafloor hydrothermal systems (Wetzel and Shock 2000). The water/rock mass ratio decreased to ~3 at the end of the experiments due to the multiple fluid samplings during the experiments.

Sampling and analytical methods

During the experiment, approximately 3–4 g of fluid samples was collected several times through a gold-lined sampling tube. For CO_2 and H_2 analyses, 0.5 mL of fluid sample was directly introduced to each Ar-purged, sealed vial at room temperature. Especially, for the CO_2 analysis, the sampled fluid was acidified (pH <2) by adding HCl to ensure the complete extraction of the dissolved bicarbonate and carbonate ions. Quantitative analysis for gas species was conducted by gas chromatography. The overall detection precision for the analyses of ΣCO_2 and H_2 concentrations in the fluid were both better than 5%. For the analysis of other dissolved species, 0.2 mL of the fluid was collected in two vials, to which either HNO_3 or NaOH was immediately added to avoid the precipitation of transition metals (Fe and Mn) and silicic acid species, respectively. The fluid samples were analyzed using inductively coupled plasma optical emission spectrometry and ion chromatography. The analytical precision (2σ) was approximately 2% for Cl and Na, and 5% for the other elements.

The pH of the fluid samples was determined using a pH meter at 25 °C under atmospheric conditions. The significant digits and precision of the pH measurement are 2 digits and ±0.1 units. This measurement was performed 1 h after sampling to allow the stabilization of the pH against CO_2 degassing. The $pH_{25\ °C}$ of the fluid cannot be measured directly because it rapidly changes due to CO_2 degassing after the sampling of fluid from the reactor. The amount of degassed CO_2 was determined from the ΣCO_2 concentrations of the fluid sample directly introduced into the sealed vial and of the fluid degassed under atmospheric conditions, then the original $pH_{25\ °C}$ was calculated based on the amount of degassed CO_2. We calculated $pH_{in\text{-}situ}$ of the high-temperature fluid in the reaction cell with the Geochemist's Workbench computer code (Bethke 2008) based on the pH at room temperature ($pH_{25\ °C}$) and concentrations of dissolved elements/species and gases. In the $pH_{in\text{-}situ}$ calculations, charge balance was constrained by $pH_{25\ °C}$, while Na was used to compensate for imbalanced charges derived from analytical errors. The required thermodynamic database was generated by the SUPCRT92 computer program (Johnson et al. 1992), using thermodynamic data of minerals, aqueous species, and complexes reported in Shock and Helgeson (1988), Shock and Koretsky (1995), Shock et al. (1989, 1997), Sverjensky et al. (1997), and McCollom and Shock (1997). The B-dot activity model was used in the calculations (Helgeson 1969; Helgeson and Kirkham 1974). The temperature-dependent activity coefficient for aqueous CO_2 was derived from the empirical relationship established by Drummond (1981), and the temperature-dependent activity of water in NaCl solution was derived from the formulation of Bethke (2008). Cleverley and Bastrakov (2005) provided useful temperature-dependent polynomial functions for both of these last-mentioned parameters.

After the experiments, alteration products were retrieved from the reaction cell and dried at 80 °C for 12 h. The solid alteration product of each experiment was analyzed with XRD and EPMA to determine the assemblage and composition of the alteration minerals. Powdery alteration products from the experiments at both temperatures were embedded in Epofix resin, and thin sections were made of these. The analytical conditions of the EPMA were 15 kV of accelerating voltage, 10 nA of specimen current, and 60–80 s of counting time. The precision of the elemental concentration was less than 10%, which was based on duplicate measurements. The detection limit for the elemental concentration was 0.01 wt.%. Moreover, the starting solid material (unaltered komatiite) was analyzed with XRD, XRF, and EPMA.

Results and Discussion

Fluid chemistry

The Cl concentration in the fluid was kept relatively constant throughout both experiments because Cl-bearing minerals are generally rare in hydrothermally altered rocks (Fig. 3 and Table 2). In contrast, the concentrations of all other components (Na, K, Mg, Ca, Si, Fe, Mn, and ΣCO_2) changed immediately after the beginning of the experiments and reached a near steady state within 2760 h at 250 °C and 1530 h at 350 °C. The Mg concentration in Exp-250 (36–40 mmol/kg) was 30–40 times higher than that in Exp-350 (<1.2 mmol/kg). The Fe concentration in Exp-250 (0.49–0.97 mmol/kg) was approximately half than that in Exp-350 (1.53–1.80 mmol/kg). No large difference between Exp-250 and Exp-350 was identified in the concentrations of other dissolved elements. Na (820–1036 mmol/kg across both experiments) had the second highest concentration next to Cl. The concentration of Ca increased and converged at 39–49 mmol/kg in Exp-250 and 37–42 mmol/kg in Exp-350. The concentrations of Si and K were 1.6–6.1 and 0.78–1.24 mmol/kg, respectively, across both experiments. The concentration of Mn was the lowest among all analyzed elements (0.15–0.73 mmol/kg across both experiments).

The ΣCO_2 concentration decreased from ca. 400 mmol/kg at the beginning of the experiments to approximately

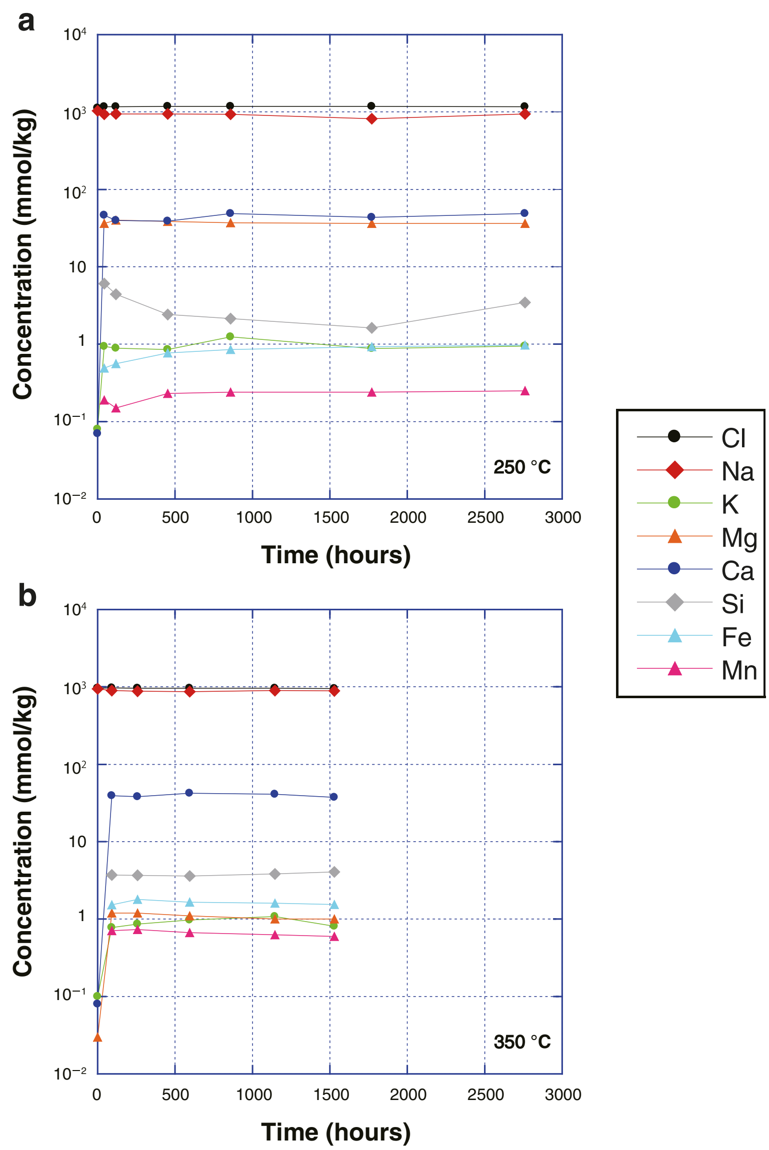

Fig. 3 Concentrations of the dissolved species in an aqueous fluid coexisting with komatiite powder and its alteration products as a function of reaction time in the experiments at **a** 250 and **b** 350 °C, 500 bars

33 mmol/kg in Exp-250 and approximately 171 mmol/kg in Exp-350 (Fig. 4a and Table 2). This trend of the steady-state ΣCO_2 concentration in the higher-temperature experiment being higher than that in the lower-temperature experiment is consistent with the results of experiments simulating high-temperature reactions between basalt and CO_2-rich seawater (Shibuya et al. 2013b). On the other hand, the $pH_{in\text{-}situ}$ values were higher than the $pH_{25\ °C}$ values at the beginning of the experiments due to the temperature dependence of the ion product of water and speciation of CO_2 species (e.g., Shibuya et al. 2010). As the reaction proceeded, the $pH_{in\text{-}situ}$ values finally decreased to 4.8 in Exp-250 and 5.7 in Exp-350, which are broadly consistent with those of high-temperature hydrothermal fluids in modern oceans ($pH_{in\text{-}situ}$ = approximately 5) (Seyfried et al. 1991).

In both experiments, the H_2 concentration in the fluid suddenly increased and temporarily reached a high value just after the start of the experiments, then slightly decreased in each experiment (Fig. 4b). Subsequently, the H_2 concentration remained almost constant in Exp-350, whereas it gradually increased with time in Exp-250. Finally, it converged to reach a steady state at up to 0.024 mmol/kg in Exp-250 and 2.9 mmol/kg in Exp-350 (Table 2). This trend indicates that the H_2 concentration was unstable due to extensive water/rock reactions just

Table 2 Composition of the sampled fluids in the experiments (mmol/kg)

Experiment	Time (h)	$pH_{25\ °C}$[a]	ΣCO_2[b]	$pH_{25\ °C}$[c]	$pH_{in\text{-}situ}$[d]	H_2	ΣCO_2	Cl	Na	K	Mg	Ca	Si	Fe	Mn
250 °C	0	n.a.	n.a.	4.9	6.0	0.003	396	1128	1036	0.08	n.d.	0.073	n.d.	n.d.	n.d.
	43	6.3	0.9	3.7	4.1	0.010	161	1174	939	0.94	36.2	46.5	6.1	0.49	0.19
	119	5.8	1.9	4.1	4.5	0.014	67	1168	951	0.89	40.4	39.7	4.4	0.56	0.15
	452	6.6	1.0	4.3	4.7	0.004	35	1186	948	0.85	38.4	39.2	2.4	0.77	0.23
	859	6.4	2.3	4.6	5.0	0.007	36	1178	937	1.24	37.2	48.7	2.1	0.85	0.24
	1771	7.1	1.0	4.4	4.8	0.021	35	1186	820	0.88	36.4	43.6	1.6	0.93	0.24
	2760	6.8	1.2	4.5	4.8	0.024	33	1175	949	0.95	36.4	48.8	3.5	0.97	0.25
350 °C	0	n.a.	n.a.	4.9	7.2	n.d.	396	966	946	0.10	0.03	0.078	n.d.	n.d.	n.d.
	90	6.1	1.9	3.8	5.6	6.0	176	971	902	0.78	1.2	39.4	3.7	1.53	0.71
	258	6.4	1.7	3.9	5.6	2.8	163	968	882	0.86	1.2	38.0	3.7	1.80	0.73
	594	6.4	1.7	3.9	5.6	2.9	179	963	877	0.98	1.1	42.2	3.6	1.65	0.67
	1146	6.5	1.8	3.9	5.7	2.7	174	969	900	1.08	1.0	41.1	3.8	1.61	0.63
	1530	6.6	1.7	3.9	5.7	2.2	171	953	884	0.81	1.0	37.3	4.1	1.55	0.60

n.a., not analyzed
n.d., not detected
[a]Measured pH after CO_2 degassing
[b]Measured ΣCO_2 concentration after CO_2 degassing
[c]Calculated $pH_{25\ °C}$ at 1 bar before CO_2 degassing at room temperature
[d]Calculated $pH_{in\text{-}situ}$ at high-temperatures, 500 bars

after the start of the experiments, and then gradually reached a steady state. The steady-state H_2 concentration in Exp-350 was approximately 100 times higher than that in Exp-250, thus indicating that differences in temperature significantly affect hydrogen generation during water-rock reactions.

Alteration products

The XRD analysis revealed that the synthetic komatiites were extensively altered throughout the experiments (Fig. 5). The results show that the alteration product in Exp-250 contains dolomite, serpentine, and a smectite/chlorite mixture (Fig. 5b), whereas calcite, serpentine, and a smectite/chlorite mixture were present as major alteration minerals in Exp-350 (Fig. 5c). The existence of serpentine and carbonate minerals in the run products indicated komatiite was altered by both serpentinization and carbonation. The precipitated carbonate mineral differed for the two temperatures.

Secondary electron imaging (SEI) and EPMA spot analysis provided more detailed information on mineral assemblage and composition (Fig. 6 and Table 3). In Exp-250, EPMA analyses of the products revealed that dolomite crystals contained a relatively high content of iron (3–9 wt.% FeO_{total}), whereas the serpentine and smectite/chlorite mixture had FeO_{total} contents of 13–15.5 wt.% (Fig. 6a–d; Table 3). Siderite (including approximately 40 wt.% FeO_{total}) and olivine were present as minor minerals in the alteration products in Exp-250 (Fig. 6a, c; Table 3). In Exp-350, the EPMA analyses of the alteration products revealed that calcite crystals had a relatively low FeO_{total} content (0.1–0.8 wt.%) and that the serpentine and smectite/chlorite mixture had FeO_{total} contents of 14–17 wt.% (Fig. 6e; Table 3). Olivine and magnetite were also identified as minor minerals; however, according to the SEI observations in many places over the thin sections, their abundances were likely greater in Exp-350 than in Exp-250. Comparing the compositions of serpentine and the smectite/chlorite mixture between Exp-250 and Exp-350, no large difference in FeO_{total} content was identified. On the other hand, on average, the FeO_{total} content in Fe-bearing dolomite in Exp-250 was ten times higher than that in calcite in Exp-350 (Table 3).

Dissolved CO_2 concentration and pH

The ΣCO_2 concentrations in fluids decreased from approximately 400 to 33 mmol/kg in Exp-250 and 171 mmol/kg in Exp-350 (Fig. 4a and Table 2). These differing steady-state ΣCO_2 concentrations indicate that carbonate minerals are destabilized with increasing temperature in the komatiite-CO_2-H_2O system. This trend is consistent with previous basalt experiments under CO_2-rich conditions at 250 and 350 °C, where the final ΣCO_2 concentrations were 1 mmol/kg at 250 °C and 108 mmol/kg at 350 °C (Shibuya et al. 2013b). Comparing results for the same temperature, the ΣCO_2 concentration in our komatiite experiments is higher than that in the basalt experiments of Shibuya et al. (2013b), thus indicating that komatiite has a lesser ability than basalt to absorb CO_2 through water-rock reactions. This would be derived from the lower CaO content of

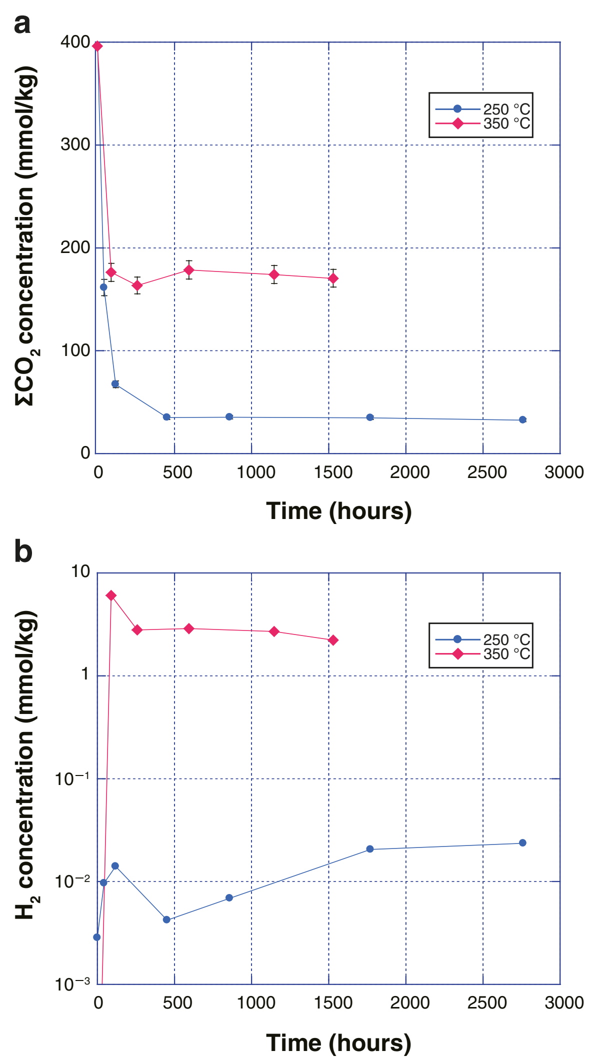

Fig. 4 Changes in **a** dissolved CO_2 and **b** H_2 concentrations in the sampled fluids as a function of reaction time

komatiite (compared with basalt) because CaO is the main component in the alteration carbonate (mainly calcite or dolomite) in the basalt and komatiite experiments (Shibuya et al. 2013b and the present study).

The final $pH_{in\text{-}situ}$ values of fluids in the present experiments ($pH_{in\text{-}situ} = 4.8$ at 250 °C and 5.7 at 350 °C) are clearly lower than those of the previous basalt-CO_2-NaCl fluid experiments ($pH_{in\text{-}situ} = 6.6$ at 250 °C and 7.2 at 350 °C) (Shibuya et al. 2013b). This discrepancy is probably derived from the lower $pH_{25\ °C}$ of the initial solution ($pH_{25\ °C} = 4.9$) in our experiments than the value of 6.5 in the basalt experiments and/or compositional differences between komatiite and basalt. In general, under CO_2-rich and near-neutral pH conditions at room temperature, substantial HCO_3^- is dissolved in the solution. With increasing temperature, the dissolved HCO_3^- is converted to $CO_{2(aq)}$ and OH^-, which elevates the $pH_{in\text{-}situ}$ value of the hydrothermal fluid (Shibuya et al. 2010). Although reactions with rocks generally cause fluid $pH_{in\text{-}situ}$ to converge near 5.5 (neutral pH at 250–350 °C), previous experiments have revealed that the alkalinization effect due to the increase in temperature under CO_2-rich conditions potentially elevates the $pH_{in\text{-}situ}$ value beyond a neutral pH value at high temperature, even if the fluid reacts with rocks (Shibuya et al. 2013b). In this study, however, the assumed $pH_{25\ °C}$ of the initial solution was 4.9, which was likely too low to form substantial HCO_3^- in the initial solution at room temperature. This implies that if seawater pH was lower than approximately 5 (CO_{2aq} was the main species), metal-rich black smoker-type hydrothermal fluids would have been generated in the Hadean komatiite hydrothermal systems in contrast to the metal-poor, alkaline hydrothermal fluids in the Archean basalt-hosted system. Although the difference in whole rock composition between komatiite and basalt should be experimentally evaluated, seawater pH was likely an important factor controlling the composition of hydrothermal fluids in the early Earth.

Serpentinization of komatiites

In this section, we compare our experimental results with conditions in natural environments and thermodynamic calculations in order to characterize the reaction occurring in the reaction cell. The EPMA analysis of alteration products revealed the presence of a small quantity of olivine in both experiments, but the amount of olivine in Exp-350 was greater than that in Exp-250. Thermodynamic calculations for serpentinization of olivine and harzburgite (80 wt.% of olivine, 15 wt.% of orthopyroxene, and 5 wt.% of clinopyroxene) indicate that olivine becomes stable and is one of the major minerals at temperatures above approximately 315–350 °C in the peridotite- or olivine-H_2O system (e.g., McCollom and Bach 2009; Klein et al. 2013). In analogy with the calculation, the experiments in this study suggest that olivine stabilizes with increasing temperature, even during komatiite serpentinization at 250–350 °C. Nevertheless, olivine was observed as a minor phase even in Exp-350. This is probably due to the composition of komatiite that contains a certain level of Al_2O_3 would stabilize serpentine and/or chlorite/smectite because smectite becomes stable as bulk Al_2O_3 content increases in ultramafic rocks such as komatiite (Shibuya et al. 2015). However, it was difficult to determine whether the igneous olivine still remains in the absence of any reaction with a fluid or if the alteration olivine was newly created through serpentinization.

Brucite commonly occurs in serpentinized rocks in modern oceanic plates (e.g., Bach et al. 2006; Klein et al.

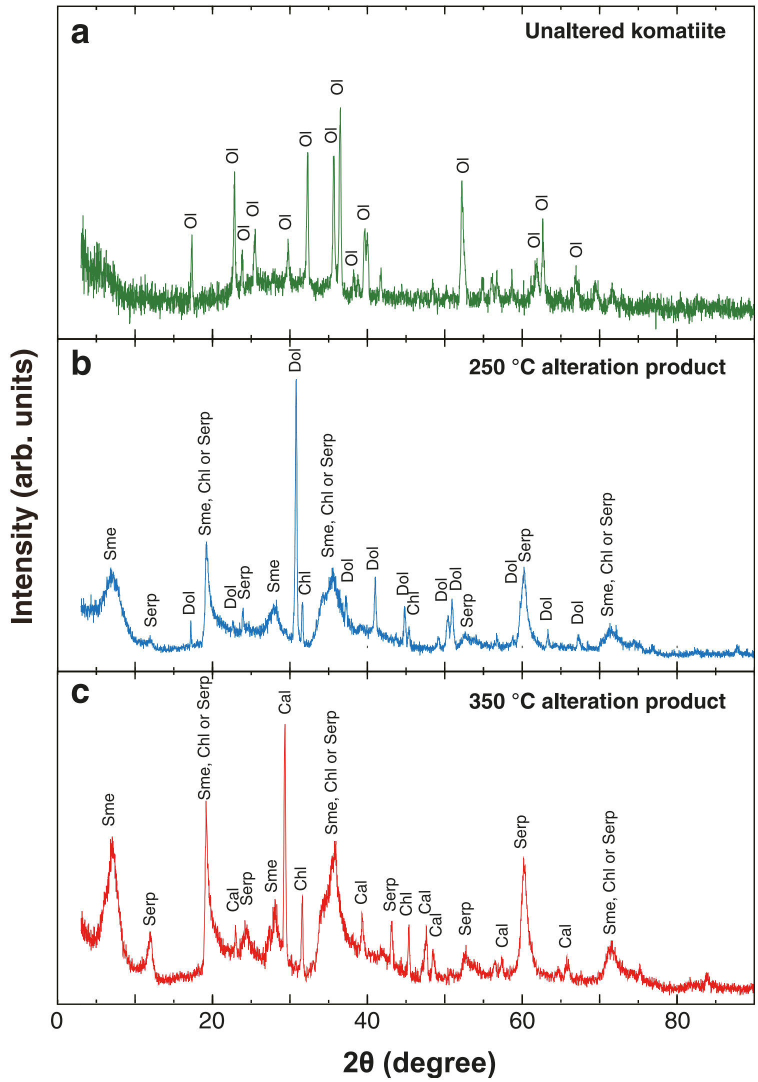

Fig. 5 Representative XRD patterns (CuKα) of **a** the unaltered synthetic komatiite and the alteration products of **b** Exp-250 and **c** Exp-350. *Dol* dolomite, *Cal* calcite, *Sme* smectite, *Chl* chlorite, *Ol* olivine, and *Serp* serpentine

2014) but was not found in the alteration products in the present experiments. The absence of brucite in Exp-350 is consistent with the thermodynamic calculations for the serpentinization of olivine and harzburgite under CO_2-poor conditions, since brucite is destabilized at temperatures above ~350 °C (McCollom and Bach 2009; Klein et al. 2013). On the other hand, the instability of brucite in Exp-250 is likely due to the CO_2-rich condition in the experiment because previous experiments revealed that Mg-bearing carbonate mineral is more stable than brucite under CO_2-rich conditions (Zhao et al. 2010; Hövelmann et al. 2012; Klein and McCollom 2013). Alternatively, high dissolved Si content in the fluid (3.7–4.1 mmol/kg) possibly prohibited brucite formation, which is supported by thermodynamic calculations (e.g., Klein and McCollom 2013).

Carbonation of komatiites

The steady-state ΣCO_2 concentrations in both experiments indicate that the amount of carbonate mineral was greater in Exp-250 than in Exp-350 (Fig. 4a and Table 2). The formation of dolomite in Exp-250 is characteristically different from the basalt-CO_2 experiments that yielded only calcite as carbonate in previous studies at 250 and 350 °C (Shibuya et al. 2013b). Comparing the experimental conditions of this study to those in the previous study, compositional differences between komatiite and basalt and/or the difference in initial pH (4.9 in this study, and 6.5 in Shibuya et al. (2013b)) likely caused the difference in precipitated carbonate species in the alteration products at 250 °C. Furthermore, it was revealed that the precipitated carbonate species strongly affected the Mg concentration in the hydrothermal fluid, i.e., Mg concentration in Exp-250

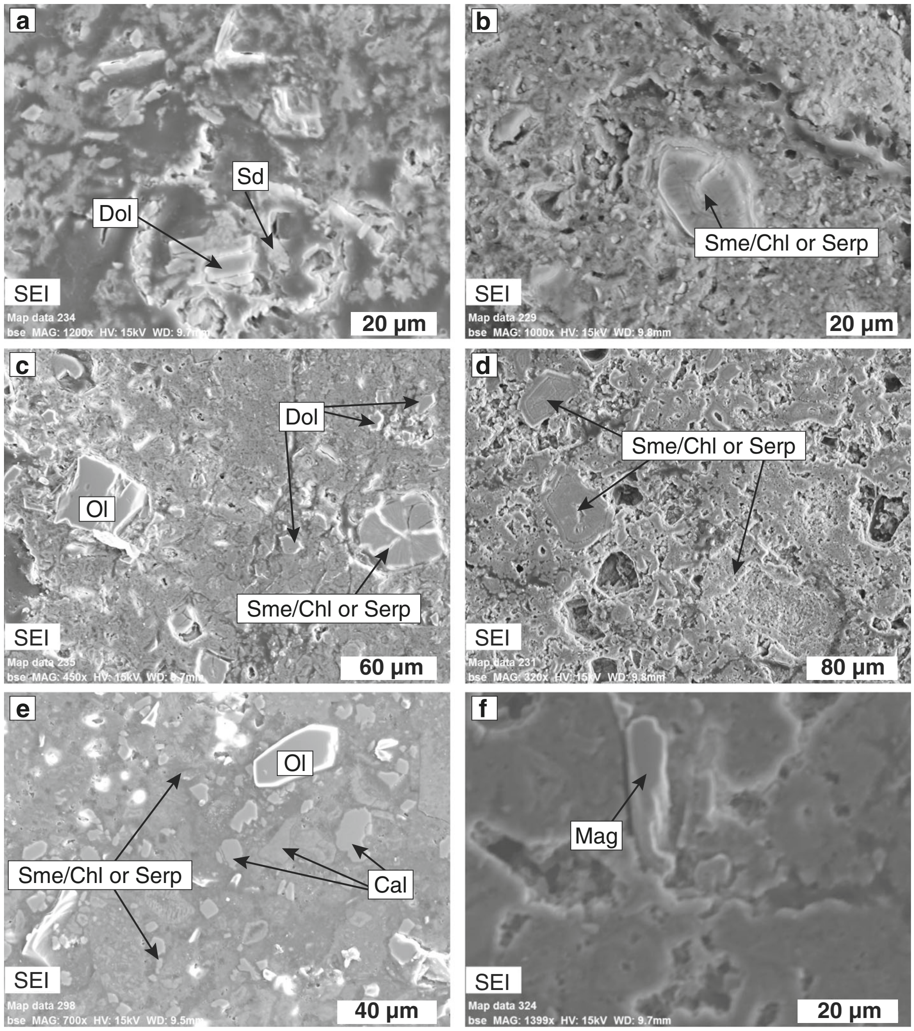

Fig. 6 Representative SEI images of alteration products (**a**–**d**) in the experiment at 250 °C and (**e**, **f**) in the experiment at 350 °C. *Sd* siderite, *Dol* dolomite, *Cal* calcite, *Sme* smectite, *Chl* chlorite, *Ol* olivine, *Serp* serpentine, and *Mag* magnetite

(carbonate as dolomite) is 30–40 times higher than that in Exp-350 (carbonate as calcite), while fluid Ca concentrations in both experiments are similar.

Previously, carbonate species were reported to correlate with the concentration ratio between Mg and Ca ($mMg^{2+}/(mMg^{2+} + mCa^{2+})$) and the temperature of the fluid (Fig. 7) (Rosenberg and Holland 1964; Rosenberg et al. 1967; Tribble et al. 1995). In Exp-350, carbonate was precipitated as calcite, whereas the $mMg^{2+}/(mMg^{2+} + mCa^{2+})$ value of the fluid was approximately 0.03; thus, it clearly falls within the stability field of calcite. On the other hand, the $mMg^{2+}/(mMg^{2+} + mCa^{2+})$ value of the fluid in Exp-250, where dolomite precipitated, was approximately 0.43, which is near the dolomite/magnesite stability boundary. Therefore, the extremely high fluid Mg concentration in Exp-250 is consistent with the precipitation of dolomite in the alteration product. However, it is difficult to discuss the anteroposterior relation between dolomite formation and enrichment of Mg in fluids because the decrease in ΣCO_2 concentration and the Mg enrichment in the fluid were already confirmed at the first sampling. It is widely accepted that seafloor hydrothermal systems play a significant role as Mg sinks in the modern ocean because basaltic oceanic crusts incorporate seawater Mg into alteration minerals such as smectite and chlorite through hydrothermal alteration at near mid-ocean ridges (e.g., Alt 1995). In addition, Charlou et al. (2002) reported that ultramafic rock-hosted high-temperature hydrothermal systems provide fluids with little Mg into seawater and generally act as Mg sinks in the ocean. On the other hand, weathering of ultramafic rocks exposed at seafloor below 150 °C and hydrothermal circulation at high water/rock ratios provide Mg into seawater (Snow and Dick 1995). Our results hypothesize that dolomite formation during the serpentinization of komatiite would be a source

Table 3 Composition of run products (wt.%)

Experiment-250 °C								Experiment-350 °C							
Sample	Serp or Sme/Chl mixture[b]			Dolomite			Siderite	Serp or Sme/Chl mixture[b]			Calcite			Olivine[c]	Magnetite
SiO_2	41.37	40.89	33.38	0.00	0.00	0.00	3.80	38.55	35.52	38.87	0.00	0.00	0.00	41.60	2.76
TiO	0.44	0.43	0.64	0.01	0.05	0.15	2.96	0.52	0.47	0.17	0.00	0.00	0.00	0.01	0.18
Al_2O_3	7.00	6.88	11.56	0.06	0.00	0.01	0.13	6.82	6.84	6.38	0.07	0.00	0.01	0.06	0.02
Cr_2O_3	0.47	0.43	0.29	0.11	0.06	0.12	1.46	0.37	0.47	0.39	0.04	0.00	0.02	0.14	0.23
FeO_{total}[a]	13.32	13.65	15.55	3.22	6.66	9.05	39.55	16.84	16.51	13.77	0.18	0.37	0.77	5.33	85.06
MnO	0.16	0.14	0.18	0.53	0.49	0.49	0.12	0.19	0.34	0.20	0.13	0.36	0.72	0.05	0.40
MgO	24.05	23.48	24.10	17.69	17.39	17.43	1.32	23.13	25.21	25.98	0.17	0.74	0.79	51.46	0.36
CaO	0.83	0.81	0.17	26.01	29.47	23.75	0.26	0.28	0.13	0.46	56.29	54.95	58.68	0.32	0.29
Na_2O	0.06	0.08	0.03	0.03	0.11	0.04	0.09	0.16	0.07	0.15	0.01	0.00	0.00	0.00	0.02
K_2O	0.09	0.11	0.02	0.03	0.02	0.02	0.05	0.04	0.01	0.03	0.01	0.01	0.01	0.02	0.03
NiO	0.17	0.20	0.12	0.00	0.00	0.08	0.10	0.10	0.00	0.16	0.01	0.00	0.05	0.45	0.10
Total	87.96	87.10	86.05	47.67	54.25	51.13	49.84	86.98	85.59	86.56	56.91	56.43	61.04	99.43	89.45
Mg# [d]	76.30	75.40	73.43	90.73	82.31	77.43	5.63	71.00	73.13	77.08	61.52	78.23	64.50	94.51	0.74

[a]Total iron as FeO
[b]Serpentine or smectite/chlorite mixture
[c]Alterlation or relict olivine
[d]Mg# = [Mg / (Mg+Fe)] × 100

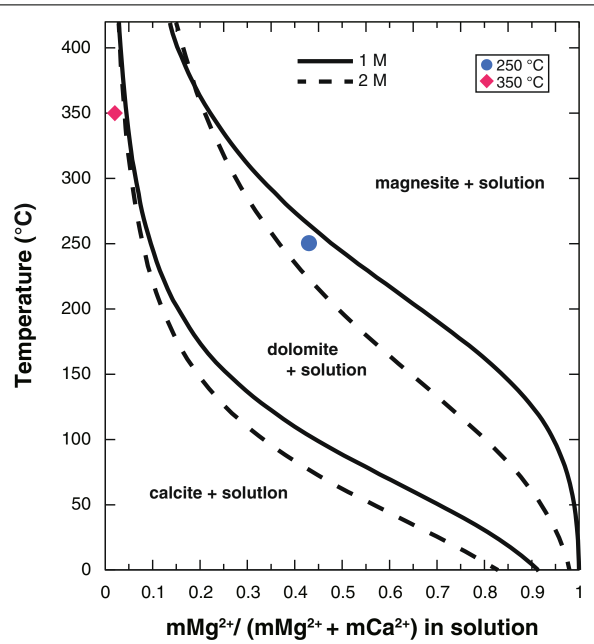

Fig. 7 The $mMg^{2+}/(mMg^{2+} + mCa^{2+})$ values of hydrothermal fluids in Exp-250 and Exp-350 plotted on the calcite-dolomite-magnesite stability fields estimated from experiments at 275–420 °C and their extrapolation to 0 °C (modified after Tribble et al. 1995). The *dotted* and *solid curves* are for the solutions with 2 and 1 M of Ca-Mg chloride, respectively. The *blue circle* and *pink diamond* indicate the values in Exp-250 and Exp-350, respectively

of Mg for the Hadean ocean, even when the temperature range of hydrothermal reaction zones was near 250 °C. Further experiments will be necessary to justify this hypothesis.

The dolomite crystals formed in this study contain up to 9 wt.% FeO_{total} in Exp-250 because Fe substitutes Mg in dolomite during its precipitation owing to the similarity in ion radius between Fe and Mg (Mg^{2+}: 0.72 Å; Fe^{2+}: 0.61 Å) (Jia 1991). A similar Fe-bearing carbonate mineral was also reported in a hydrothermal alteration experiment for komatiite conducted under CO_2-rich conditions (water 50.1 mg + CO_2 7.3 mg: about 3300 mmol/kg at the starting condition) at 300 °C and 500 bars (Hao and Li 2015). Furthermore, Klein and McCollom (2013) reported the precipitation of Fe-bearing magnesite (FeO = 6.78 wt.%) through the serpentinization of olivine under CO_2-rich conditions at 230 °C. Although differences in the composition of the starting materials between the previous studies and our experiments would have caused the difference in carbonate species, it seems likely that carbonate minerals formed during serpentinization under CO_2-rich conditions contain substantial FeO, probably at temperatures below approximately 300–350 °C.

Effect of seawater CO_2 on H_2 concentration in fluid

The maximum steady-state fluid H_2 concentrations were 0.024 mmol/kg in Exp-250 and 2.9 mmol/kg in Exp-350 (Fig. 4b), and the results are consistent with the analysis of solid alteration products. Magnetite, whose formation is related to H_2 generation (McCollom and Bach 2009), was observed in Exp-350 but not in Exp-250. Nevertheless, the H_2 concentrations in both experiments were clearly lower than the steady-state H_2 concentration (~20 mmol/kg) in fluid generated by the reactions between komatiite and a CO_2-free NaCl fluid at 300 °C and 500 bars (Shibuya et al. 2015). Although direct comparison is difficult owing to the difference in temperature conditions, two possible factors explain the differences between the previous and present experiments in terms of the steady-state H_2 concentrations from the hydrothermal reaction of komatiite.

The first factor is the temperature dependence of the stability of magnetite in ultramafic systems. At temperatures below 315–350 °C, the amount of magnetite formation increases with increasing temperature, but it drastically decreases at temperatures above 315–350 °C because olivine becomes stable (McCollom and Bach 2009; Klein et al. 2013). Moreover, Klein et al. (2013) reported that within the temperature range of 25–400 °C, the amount of hydrogen generation caused by the reaction with olivine (Fo 90) reaches a maximum at 322 °C. Thus, the temperature dependence of the stability of olivine and magnetite would be a primary cause of the difference in fluid H_2 concentrations between the previous CO_2-free komatiite experiment at 300 °C and our experiments.

The other factor is the presence of CO_2 in the experimental system. Based on thermodynamic calculations simulating the relative amount of magnetite formation at 50–400 °C under 500 bars, Klein et al. (2013) expected that the amount of hydrogen generation caused by the reaction with olivine under CO_2-free conditions is greater at 250 °C than at 350 °C. In our experiments, however, the steady-state fluid H_2 concentration was higher in Exp-350 than in Exp-250. In previous experiments that simulated the reactions between olivine and a CO_2-rich fluid at 230 °C and 35 MPa, ferrous iron-bearing talc and magnesite were generated, while magnetite formation and H_2 generation were limited (Klein and McCollom 2013). Under CO_2-free conditions, the iron is only partitioned into magnetite and ferrous iron-bearing silicate in alteration products,

$$\mathrm{a(FeO)_{rock} + bH_2O \rightarrow d(Fe_2O_3)_{rock}} + d\mathrm{H_2} + (\mathrm{a}\text{-}2d)\mathrm{(FeO)_{rock}}.$$

In contrast, the interaction between CO_2-rich fluid and rock leads to carbonate mineral precipitation and ferrous iron incorporation therein. The reaction occurring under a CO_2-rich condition is the following:

$$\mathrm{a(FeO)_{rock} + bH_2O + cCO_2 \rightarrow d(Fe_2O_3)_{rock} + dH_2 + e(FeO)_{rock}} + (\mathrm{a}\text{-}2d\text{-e})\mathrm{(FeCO_3)_{rock}} + (\mathrm{c\text{-}a} + 2d + \mathrm{e})\mathrm{CO_2}.$$

In both equations, the value of "d" is the amount of H_2 generation and depends on temperature. Therefore, it was suggested that the lack of H_2 generation is due to the direct incorporation of ferrous iron into carbonate minerals without its oxidation during the hydrothermal alteration. In our experiments, although a large difference in the composition of serpentine and smectite/chlorite mixture was not identified between Exp-250 and Exp-350, the Fe content of dolomite in Exp-250 (3–9 wt.% FeO_{total}) was clearly higher than that of calcite in Exp-350 (Table 3). The amount of generated magnetite in Exp-350 was greater than that in Exp-250. These data suggest that the amount of ferrous iron incorporated into the carbonate mineral strongly affected the extent of magnetite formation and resulting hydrogen generation in the fluid. Although such a trend in the effect of CO_2 on H_2 generation has been reported in some previous experiments at temperatures below 230 °C (Jones et al. 2010; Klein and McCollom 2013; Neubeck et al. 2014), our experiments show that the suppression of H_2 generation by the presence of CO_2 in the system occurs even at higher temperatures (250 °C) and in the CO_2-H_2O-komatiite system. In addition, a small amount of ferrous iron incorporated into calcite (up to 0.8 wt.%) may have also slightly suppressed magnetite formation in Exp-350.

Implications for the Hadean H_2-rich hydrothermal environments

It has been considered that the serpentinization of komatiite would have served as the most ubiquitous geological process for hosting H_2-rich hydrothermal environments in the Hadean ocean (e.g., Takai et al. 2006). The present experiments constrained the potential for H_2 generation during the serpentinization of komatiite under CO_2-rich conditions. This work provides further important insights into our interpretation of hatcheries for the emergence and early evolution of life in the Hadean Earth. Exp-350 showed that the fluid H_2 concentration increased up to 2.9 mmol/kg during the serpentinization and carbonation of komatiite. This value is lower than the maximum H_2 concentration of the vent fluids in modern peridotite-hosted hydrothermal systems; the H_2 and ΣCO_2 concentrations in modern peridotite-hosted hydrothermal systems are 12 and 10.1 mM at Logatchev field, 16 and 16 mM at Rainbow field (Charlou et al. 2002), and <1–15 mmol/kg and <0.8 mmol/kg at Lost City field (Kelley et al. 2005), respectively. However, the H_2 concentration in Exp-350 broadly falls within the range of the fluid H_2 concentrations in the Kairei field hosted by both basalt and troctolite ($H_2 = 2.5$–8.5 mmol/kg and $\Sigma CO_2 < 10.1$ mmol/kg; Takai et al. 2004; Gallant and Von Damm 2006; Kumagai et al. 2008; Nakamura et al. 2009). This suggests that in the Hadean, the komatiite still had great potential to generate H_2-rich hydrothermal fluids at high-temperature, even under CO_2-rich conditions. Furthermore, considering that hydrogenotrophic methanogens—long believed to be one of the most probable candidates for the earliest living forms and primary producers on Earth (e.g., Takai et al. 2006; Martin et al. 2008)—indeed dominate in the microbial communities associated with hydrothermal fluids in the Kairei field (Takai et al. 2004), the komatiite-hosted seafloor hydrothermal systems would have fully prepared the energetic basis of hatcheries for the emergence and early evolution of hydrogenotrophic living forms in the Hadean ocean.

In contrast, the fluid H_2 concentration in Exp-250 (0.024 mmol/kg) was much lower than that in Exp-350 and is comparable to the H_2 concentration level in the typical fluids of modern basalt-hosted hydrothermal fields (Charlou et al. 1996, 2000; Gallant and Von Damm 2006). Given that the H_2 generation potential of ultramafic rocks decreases with decreasing temperature within the unstable region of olivine (McCollom and Bach 2009; Klein et al. 2013), the serpentinization of komatiite under CO_2-rich conditions might not have afforded the H_2-rich hydrothermal fluids at temperatures lower than 250 °C. More importantly, carbonate minerals become stable with decreasing temperature in H_2O-CO_2-rock systems (e.g., Shibuya et al. 2013b), which indicates that the carbonate formation and resulting limitation of H_2 generation would occur more significantly at lower temperatures (e.g., <100 °C). Therefore, the possible H_2-rich hydrothermal environments may have been created only in the deep ocean floor because high hydrostatic pressure can elevate the temperature of hydrothermal reaction zones (fluid-rock reaction zones). In other words, other potential candidates, such as the hydrothermal systems in on-land and shallow submarine environments, may not have fully prepared the energetic basis (abundant H_2 availability) of hatcheries for the emergence and early evolution of life in the Hadean Earth due to low-temperature hydrothermal reactions.

Conclusions

High-temperature and high-pressure experiments using komatiite and a CO_2-rich NaCl solution revealed that different hydrothermal reaction temperatures caused differences in the carbonate species in alteration products (iron-rich dolomite at 250 °C and calcite at 350 °C) during the serpentinization of komatiites. The hydrothermal fluid coexisting with dolomite at 250 °C showed high Mg concentrations (up to ca. 40 mmol/kg), which is markedly higher than those in typical modern high-temperature hydrothermal fluids (generally less than 1 mmol/kg). This suggests that, in contrast to modern seafloor hydrothermal systems, the dolomite-bearing komatiite-hosted hydrothermal systems may have served as a source of Mg in the Hadean ocean. The steady-state H_2 concentration in Exp-350 (up to 2.9 mmol/kg) was approximately 100 times higher than that in Exp-250 (up to 0.024 mmol/kg) because the amount of ferrous iron incorporated into carbonate was greater in Exp-250 than in Exp-350. These results perhaps suggest that only high-temperature komatiite-hosted hydrothermal systems have the potential to generate H_2-rich hydrothermal environments, even in the CO_2-abundant Hadean ocean. Further experiments based on a more precise estimation of the ancient atmospheric/oceanic CO_2 levels from geological records will clarify the geochemical nature of komatiite-hosted hydrothermal environments and other potential hatcheries for the emergence and early evolution of life in the Hadean Earth because the ΣCO_2 concentration in the fluid may significantly affect the mineral assemblage of serpentinized komatiites and hydrothermal reactions taking place under various conditions.

Abbreviations

BSE: Backscattered electron; EPMA: Electron probe microanalyzer; Exp-250: Experiment at 250 °C; Exp-350: Experiment at 350 °C; QFM: Quartz-fayalite-magnetite; SEI: Secondary electron imaging; XRD: X-ray diffraction; XRF: X-ray fluorescence

Acknowledgements

We thank two anonymous reviewers for many helpful comments that greatly improved our manuscript. We appreciate Prof. Hodaka Kawahata for editorial handling. We are grateful to Y. Ueno for discussions.

Funding

This work was supported by Grants-in-Aid for Scientific Research from the Japan Society for Promotion of Science (JSPS) (No. 15K13583) and the Ministry of Education, Culture, Sports, Science and Technology (MEXT), Japan.

Authors' contributions

HU, TS, KT, and SM proposed and designed the study. HU and TS carried out the experiments. HU, TS, and MS prepared the starting materials. HU, TS, MS, and YS analyzed the fluid samples and solid materials. All authors interpreted the data, read, and approved the final manuscript.

Competing interests

The authors declare that they have no competing interests.

Author details

[1]Department of Earth and Planetary Sciences, Tokyo Institute of Technology, 2-12-1 Ookayama, Meguro-ku, Tokyo 152-8551, Japan. [2]Laboratory of Ocean-Earth Life Evolution Research (OELE), Japan Agency for Marine-Earth Science and Technology (JAMSTEC), 2-15 Natsushima-cho, Yokosuka 237-0061, Japan. [3]Research and Development Center for Submarine Resources, Japan Agency for Marine-Earth Science and Technology (JAMSTEC), 2-15 Natsushima-cho, Yokosuka 237-0061, Japan. [4]Project Team for Development of New-generation Research Protocol for Submarine Resources, Japan Agency for Marine-Earth Science and Technology (JAMSTEC), 2-15 Natsushima-cho, Yokosuka 237-0061, Japan. [5]Department of Subsurface Geobiological Analysis and Research (SUGAR), Japan Agency for Marine-Earth Science and Technology (JAMSTEC), 2-15 Natsushima-cho, Yokosuka 237-0061, Japan. [6]Earth-Life Science Institute (ELSI), Tokyo Institute of Technology, 2-12-1 Ookayama, Meguro-ku, Tokyo 152-8551, Japan.

Received: 22 March 2016 Accepted: 21 October 2016
Published online: 18 November 2016

References

Allen DE, Seyfried WE (2003) Compositional controls on vent fluids from ultramafic-hosted hydrothermal systems at mid-ocean ridges: an experimental study at 400 °C, 500 bars. Geochim Cosmochim Acta 67:1531–1542

Alt JC (1995) Subseafloor processes in mid-oceanic ridge hydrothermal systems. In: Humphris SE, Zierenberg RA, Mullineaux LS, Thomson RE (eds) Seafloor hydrothermal systems: physical, chemical, biological, and geological interactions. Geophysical monograph. American Geophysical Union, Washington, DC, pp 85–114

Amend JP, McCollom TM (2009) Energetics of biomolecule synthesis on early Earth. In: Zaikowski L, Friedrich JM, Seidel SR (eds) Chemical evolution II: from the origins of life to modern society. American Chemical Society, Washington, DC, pp 63–94

Bach W, Paulick H, Garrido CJ, Ildefonse B, Meurer WP, Humphris SE (2006) Unraveling the sequence of serpentinization reactions: petrography, mineral chemistry, and petrophysics of serpentinites from MAR 15°N (ODP Leg 209, Site 1274). J Geophys Res 33, L13306. doi:10.1029/12006GL025681

Bethke CM (2008) Geochemical and biogeochemical reaction modeling. Cambridge Univ. Press, Cambridge, U. K

Canil D (1997) Vanadium partitioning and the oxidation state of Archaean komatiite magma. Nature 389:842–845

Charlou JL, Donval JP, Douville E, Jean-Baptiste P, Radford-Knoery J, Fouquet Y, Dapoigny A, Stievenard M (2000) Compared geochemical signatures and the evolution of Menez Gwen (37°50′N) and Lucky Strike (37°17′N) hydrothermal fluids, south of the Azores Triple Junction on the Mid-Atlantic Ridge. Chem Geol 171:49–75

Charlou JL, Donval JP, Fouquet Y, Jean-Baptiste P, Holm N (2002) Geochemistry of high H_2 and CH_4 vent fluids issuing from ultramafic rocks at the Rainbow Hydrothermal Field (36°14′N, MAR). Chem Geol 191:345–359

Charlou JL, Donval JP, Jean-Baptiste P, Dapoigny A, Rona PA (1996) Gases and helium isotopes in high temperature solutions sampled before and after ODP Leg 158 Drilling at TAG Hydrothermal Field (26° N, MAR). Geophys Res Lett 23:3491–3494

Cleverley JS, Bastrakov EN (2005) K2GWB: utility for generating thermodynamic data files for The Geochemist's Workbench® at 0-1000 °C and 1-5000 bar from UT2K and the UNITHERM database. Comput Geosci 31(6):756–767

Drummond SE (1981) Boiling and mixing of hydrothermal fluids: chemical effects on mineral precipitation. Dissertation, Pennsylvania State University

Gallant RM, Von Damm KL (2006) Geochemical controls on hydrothermal fluids from the Kairei and Edmond Vent Fields, 23°–25°S, Central Indian Ridge. Geochem Geophys Geosyst 7, Q06018. doi:10.1029/2005GC001067

Hao X, Li Y (2015) Hexagonal plate-like magnetite nanocrystals produced in komatiite-H_2O-CO_2 reaction system at 450 °C. Int J Astrobiol 14:547–553

Helgeson HC (1969) Thermodynamics of hydrothermal systems at elevated temperatures and pressures. Am J Sci 267:729–804

Helgeson HC, Kirkham DH (1974) Theoretical prediction of the thermodynamic behavior of aqueous electrolytes at high pressures and temperatures: II. Debye–Huckel parameters for activity coefficients and relative partial molal properties. Am J Sci 274:1199–1261

Hövelmann J, Putnis CV, Ruiz-Agudo E, Austrheim H (2012) Direct nanoscale observations of CO_2 sequestration during brucite [$Mg(OH)_2$] dissolution. Environ Sci Technol 46:5253–5260

Jia YQ (1991) Crystal radii and effective ionic radii of the rare earth ions. Journal of Solid State Chemistry 95:184–187

Johnson JW, Oelkers EH, Helgeson HC (1992) SUPCRT92: a software package for calculating the standard molal thermodynamic properties of minerals gases, aqueous species, and reactions from 1 to 5000 bar and 0 to 1000 °C. Comput Geosci 18:899–947

Jones LC, Rosenbauer R, Goldsmith JI, Oze C (2010) Carbonate control of H_2 and CH_4 production in serpentinization systems at elevated P-Ts. Geophys Res Lett 37, L14306

Kasting JF (1993) Earth's early atmosphere. Science 259(5097):920–926

Kelley DS, Karson JA, Fruh-Green GL, Yoerger DR, Shank TM, Butterfield DA, Hayes JM, Schrenk MO, Oison EJ, Proskurowski G, Jakuba M, Bradley A, Larson B, Ludwig K, Glickson D, Buckman K, Bradley AS, Brazelton WJ, Roe K, Elend MJ, Delacour A, Bernasconi SM, Lilley MD, Baross JA, Summons RE, Sylva SP (2005) A serpentinite-hosted ecosystem: the lost city hydrothermal field. Science 307:1428–1434

Klein F, McCollom TM (2013) From serpentinization to carbonation: new insights from a CO_2 injection experiment. Earth Planet Sci Lett 379:137–145

Klein F, Bach W, McCollom TM (2013) Compositional controls on hydrogen generation during serpentinization of ultramafic rocks. Lithos 178:55–69

Klein F, Bach W, Humphris SE, Kahl W-A, Jöns N, Moskowitz B, Berquó TS (2014) Magnetite in seafloor serpentinite—some like it hot. Geology 42:135–138

Knauth LP (2005) Temperature and salinity history of the Precambrian ocean: implications for the course of microbial evolution. Palaeogeogr Palaeoclimatol Palaeoecol 219:53–69

Komiya T, Maruyama S, Hirata T, Yurimoto H (2002) Petrology and geochemistry of MORB and OIB in the Mid-Archean North Pole region, Pilbara Craton, Western Australia, implications for the composition and temperature of the upper mantle at 3.5 Ga. Int Geol Rev 44:988–1016

Komiya T (2004) Material circulation model including chemical differentiation within the mantle and secular variation of temperature and composition of the mantle. Phys Earth Planet Int 146:333–367

Kumagai H, Nakamura K, Toki T, Morishita T, Okino K, Ishibashi JI, Tsunogai U, Kawagucci S, Gamo T, Shibuya T, Sawaguchi T, Neo N, Joshima M, Sato T, Takai K (2008) Geological background of the Kairei and Edmond hydrothermal fields along the Central Indian Ridge: implications of their vent fluids' distinct chemistry. Geofluids 8:239–251

Kump LR, Seyfried WE (2005) Hydrothermal Fe fluxes during the Precambrian: effect of low oceanic sulfate concentrations and low hydrostatic pressure on the composition of black smokers. Earth Planet Sci Lett 235:654–662

Lazar C, McCollom TM, Manning CE (2012) Abiogenic methanogenesis during experimental komatiite serpentinization: implications for the evolution of the early Precambrian atmosphere. Chem Geol 326–327:102–112

Lowe DR, Tice MM (2004) Geologic evidence for Archean atmospheric and climatic evolution: fluctuating levels of CO_2, CH_4, and O_2 with an overriding tectonic control. Geology 32:493–496

Martin W, Baross J, Kelley D, Russell MJ (2008) Hydrothermal vents and the origin of life. Nat Rev Microbiol 6:805–814

Macleod G, McKeown C, Hall AJ, Russell MJ (1994) Hydrothermal and oceanic pH conditions of possible relevance to the origin of life. Orig Life Evol Biosph 24:19–41

McCollom TM, Bach W (2009) Thermodynamic constraints on hydrogen generation during serpentinization of ultramafic rocks. Geochim Cosmochim Acta 73:856–875

McCollom TM, Shock EL (1997) Geochemical constraints on chemolithoautotrophic metabolism by microorganisms in seafloor hydrothermal systems. Geochim Cosmochim Acta 61:4375–4391

Moores EM (2002) Pre-1 Ga (pre-Rodinian) ophiolites: their tectonic and environmental implications. GSA Bulletin 114:80–95

Nakamura K, Morishita T, Bach W, Klein F, Hara K, Okino K, Takai K, Kumagai H (2009) Serpentinized troctolites exposed near the Kairei hydrothermal field Central Indian Ridge: insights into the origin of the Kairei hydrothermal fluid supporting a unique microbial ecosystem. Earth Planet Sci Lett 280:128–136

Nakamura K, Takai K (2014) Theoretical constraints of physical and chemical properties of hydrothermal fluids on variations in chemolithotrophic microbial communities in seafloor hydrothermal systems. Progr Earth Planet Sci 1(1):1–24

Neubeck A, Duc NT, Hellevang H, Oze C, Bastviken D, Bacsik Z, Holm NG (2014) Olivine alteration and H_2 production in carbonate-rich, low temperature aqueous environments. Planet Space Sci 96:51–61

Ohmoto H, Watanabe Y, Kumazawa K (2004) Evidence from massive siderite beds for a CO_2-rich atmosphere before ~1.8 billion years ago. Nature 429:395–399

Ohta H, Maruyama S, Takahashi E, Watanabe Y, Kato Y (1996) Field occurrence, geochemistry and petrogenesis of the Archean mid-oceanic ridge basalts (AMORBs) of the Cleaverville area, Pilbara Craton, Western Australia. Lithos 37:199–221

Rosenberg PE, Holland HD (1964) Calcite-dolomite-magnesite stability relations in solutions at elevated temperatures. Science 145:700–701

Rosenberg PE, Burt DM, Holland HD (1967) Calcite-Dolomite-Magnesite stability relations in solutions: the effect of ionic strength. Geochim Cosmochim Acta 31:391–396

Russell MJ, Barge LM, Bhartia R, Bocanegra D, Bracher PJ, Branscomb E, Kidd R, McGlynn S, Meier DH, Nitschke W, Shibuya T, Vance S, White L, Kanik I (2014) The drive to life on wet and icy worlds. Astrobiology 14:308–343

Russell MJ, Hall AJ (1997) The emergence of life from iron monosulphide bubbles at a submarine hydrothermal redox and pH front. J Geol Soc Lond 154:377–402

Russell MJ, Hall AJ, Martin W (2010) Serpentinization as a source of energy at the origin of life. Geobiology 8:355–371

Seyfried WE, Ding K, Berndt ME (1991) Phase equilibria constraints on the chemistry of hot spring fluids at mid-ocean ridges. Geochim Cosmochim Acta 55:3559–3580

Seyfried WE, Gordon PC, Dickson FW (1979) A new reaction cell for hydrothermal solution equipment. Am Mineral 64:646–649

Seyfried WE, Foustoukos DI, Fu Q (2007) Redox evolution and mass transfer during serpentinization: an experimental and theoretical study at 200 °C, 500 bar with implications for ultramafic-hosted hydrothermal systems at mid-ocean ridges. Geochim Cosmochim Acta 71:3872–3886
Shibuya T, Kitajima K, Komiya T, Terabayashi M, Maruyama S (2007) Middle Archean ocean ridge hydrothermal metamorphism and alteration recorded in the Cleaverville area, Pilbara Craton, Western Australia. J Metamorph Geol 25:751–767
Shibuya T, Komiya T, Nakamura K, Takai K, Maruyama S (2010) Highly alkaline, high-temperature hydrothermal fluids in the early Archean ocean. Precambrian Res 182:230–238
Shibuya T, Russell MJ, Takai K (2016) Free energy distribution and hydrothermal mineral precipitation in Hadean submarine alkaline vent systems: Importance of iron redox reactions under anoxic conditions. Geochim Cosmochim Acta 175:1–19
Shibuya T, Tahata M, Kitajima K, Ueno Y, Komiya T, Yamamoto S, Igisu M, Terabayashi M, Sawaki Y, Takai K, Yoshida N, Maruyama S (2012) Depth variation of carbon and oxygen isotopes of calcites in Archean altered upper oceanic crust: implications for the CO_2 flux from ocean to oceanic crust in the Archean. Earth Planet Sci Lett 321–322:64–73
Shibuya T, Tahata M, Ueno Y, Komiya T, Takai K, Yoshida N, Maruyama S, Russell MJ (2013a) Decrease of seawater CO_2 concentration in the Late Archean: an implication from 2.6 Ga seafloor hydrothermal alteration. Precambrian Res 236:59–64
Shibuya T, Yoshizaki M, Masaki Y, Suzuki K, Takai K, Russell MJ (2013b) Reactions between basalt and CO_2-rich seawater at 250 and 350 °C, 500 bars: implications for the CO_2 sequestration into the modern oceanic crust and the composition of hydrothermal vent fluid in the CO_2-rich early ocean. Chem Geol 359:1–9
Shibuya T, Yoshizaki M, Satoh M, Shimizu K, Nakamura K, Omori S, Suzuki K, Takai K, Hideo T, Maruyama S (2015) Hydrogen-rich hydrothermal environments in the Hadean ocean inferred from serpentinization of komatiites at 300 °C and 500 bar. Progr Earth Planet Sci 2:1–11. doi:10.1186/s40645-015-0076-z
Shock EL, Koretsky CM (1995) Metal-organic complexes in geochemical processes: estimation of standard partial molal thermodynamic properties of aqueous complexes between metal cations and monovalent organic acid ligands at high pressures and temperatures. Geochim Cosmochim Acta 59:1497–1532
Shock EL, Helgeson HC (1988) Calculation of the thermodynamic and transport properties of aqueous species at high pressures and temperatures: correlation algorithms for ionic species and equation of state predictions to 5 kb and 1000 °C. Geochim Cosmochim Acta 52:2009–2036
Shock EL, Helgeson HC, Sverjensky DA (1989) Calculation of the thermodynamic and transport properties of aqueous species at high pressures and temperatures: standard partial molal properties of inorganic neutral species. Geochim Cosmochim Acta 53:2157–2183
Shock EL, Sassani DC, Willis M, Sverjensky DA (1997) Inorganic species in geologic fluids: correlations among standard molal thermodynamic properties of aqueous ions and hydroxide complexes. Geochim Cosmochim Acta 61:907–950
Sleep NH, Zahnle K (2001) Carbon dioxide cycling and implications for climate on ancient Earth. J Geophys Res 106:1373–1399
Smith HS, Erlank AJ, Duncan AR (1980) Geochemistry of some ultramafic komatiite lava flows from the Barberton Mountain Land, South Africa. Precambrian Res 11:399–415
Snow JE, Dick HJB (1995) Pervasive magnesium loss by marine weathering of peridotite. Geochim Cosmochim Acta 59:4219–4235
Suzuki K, Shibuya T, Yoshizaki M, Hirose T (2015) Experimental hydrogen production in hydrothermal and fault systems: significance for habitability of subseafloor H_2 chemoautotroph microbial ecosystems. In: Ishibashi J, Okino K, Sunamura M (eds) Subseafloor biosphere linked to hydrothermal systems. TAIGA concept. Springer, Tokyo, pp 87–94
Sverjensky DA, Shock EL, Helgeson HC (1997) Prediction of the thermodynamic properties of aqueous metal complexes to 1000 °C and 5 kb. Geochim Cosmochim Acta 61:1359–1412
Takai K, Gamo T, Tsunogai U, Nakayama N, Hirayama H, Nealson KH, Horikoshi K (2004) Geochemical and microbiological evidence for a hydrogen-based, hyperthermophilic subsurface lithoautotrophic microbial ecosystem (HyperSLiME) beneath an active deep-sea hydrothermal field. Extremophiles 8:269–282
Takai K, Nakamura K, Suzuki K, Inagaki F, Nealson KH, Kumagai H (2006) Ultramafics-hydrothermalism-hydrogenesis-hyperslime (ultra H^3) linkage: a key insight into early microbial ecosystem in the Archean deep-sea hydrothermal systems. Paleontol Res 10:269–282
Tribble JS, Arvidson RS, Lane M, Mackenzie FT (1995) Crystal chemistry, and thermodynamic and kinetic properties of calcite, dolomite, apatite, and biogenic silica: applications to petrographic problems. Sediment Geol 95:11–51
Walker JCG (1985) Carbon dioxide on the early earth. Orig Life Evol Biosph 16:117–127
Wei K, Tronnes RG, Scarfe CM (1990) Phase relations of aluminum-undepleted and aluminum-depleted komatiites at pressures of 4–12 GPa. J Geophys Res 95:15817–15827
Wetzel LR, Shock EL (2000) Distinguishing ultramafic- from basalt-hosted submarine hydrothermal systems by comparing calculated vent fluid compositions. J Geophys Res 105:8319–8340
Yanagawa H, Kojima K (1985) Thermophilic microspheres of peptide-like polymers and silicates formed at 250 °C. J Biochem 97:1521–1524
Yoshizaki M, Shibuya T, Suzuki K, Shimizu K, Nakamura K, Takai K, Omori S, Maruyama S (2009) H_2 generation by experimental hydrothermal alteration of komatiitic glass at 300 °C and 500 bars: a preliminary result from on-going experiment. Geochem J 43:e17–e22
Zhao L, Sang L, Chen J, Ji JF, Teng HH (2010) Aqueous carbonation of natural brucite: relevance to CO_2 sequestration. Environ Sci Technol 44:406–411